Int. J. Heat Mass Transfer. Vol. 34, No. 6, pp. 1429–1442, 1991
Printed in Great Britain

0017–9310/91 $3.00 + 0.00

Transient laminar natural convection from horizontal cylinders

P. WANG,† R. KAHAWITA† and D. L. NGUYEN†‡

† Department of Civil Engineering, Ecole Polytechnique de Montréal, Montréal, Québec, H3C 3A7, Canada
‡ VP Recherche, Hydro-Québec, Varennes, Québec, J3X 1S1, Canada

(*Received* 11 *December* 1989 *and in final form* 6 *July* 1990)

Abstract—The unsteady laminar natural convection flow from a heated horizontal cylinder under diverse surface boundary conditions is investigated numerically using the spline fractional step method. Some characteristics of the boundary layer obtained with a scale analysis are compared with the numerical results. The development of the plume region as well as the surface heat transfer and local flow field are evaluated. At small times, the present numerical solutions approach the boundary layer results and are in good agreement with the results from the scale analysis. A more detailed study of the development of the plume region, using computed particle trajectories is reported. All results are obtained using a personal computer. Qualitative comparisons between the present results and flow visualization experiments partially verify the numerical results.

INTRODUCTION

TWO-DIMENSIONAL laminar natural convection from horizontal cylinders has been extensively investigated analytically, numerically and experimentally. Most prior work has concentrated on steady-state situations with either a specified surface temperature or a uniform surface heat flux. Thus Kuehn and Goldstein [1] numerically solved the complete Navier–Stokes and energy equations for laminar natural convection from a horizontal isothermal cylinder using a finite-difference technique. Farouk and Guceri [2] attacked the same problem for uniform as well as non-uniform surface temperature and heat flux distributions on the cylinder. Qureshi and Ahmad [3] provided numerical solutions for a horizontal cylinder with uniform heat flux using a technique similar to that indicated in ref. [1]. The authors [4] recently reported on an extensive numerical study of the laminar natural convection flow from a heated horizontal cylinder using a newly developed spline fractional step technique [5].

The literature on transient free convection studies is much less abundant. The great majority of studies reported in the literature are concerned with geometries such as vertical cylinders or plates. Typically, an initially pure conduction situation is followed by a convective transition regime in which leading edge effects become dominant. Finally, a transient approach to a steady state occurs. Unsteady natural convection from a horizontal cylinder has not been extensively treated. A perusal of the current literature on the subject indicates that very few studies have been realized in which an attempt is made to define the typical characteristics of the problem. An experimental study by Ostroumov [6] reported on the development of the convection regime initiated by a suddenly heated fine wire. Vest and Lawson [7] also reported on a similar experiment. Parsons and Mulligan [8] presented experimental data for the transient free convective heat transfer from a horizontal wire in air. An early analytical study, using the boundary layer approximation and series continuation for small time was established by Elliott [9]. He considered large Grashof numbers and derived solutions for the stream function and the temperature field. Values of the skin friction and heat transfer coefficient obtained for small time were then extrapolated to infinite time to predict their final steady-state values. These results are of course, invalid in the plume region where the boundary layer assumption breaks down. Based on ref. [9], Gupta and Pop [10] performed a perturbation analysis of the boundary layer equations for the unsteady free convection past a circular cylinder in order to estimate the influence of curvature effects on the surface heat transfer as well as on the skin friction. Their results indicated that the curvature leads to an increase in both skin friction and heat transfer rate from the surface of the cylinder. In a study similar to that of ref. [8], Katagiri and Pop [11] reported numerical solutions to the unsteady free convection for an isothermal horizontal cylinder the temperature of which is suddenly increased to a large Grashof number. Sako *et al.* [12] presented numerical solutions to the transient natural convection from a horizontal cylinder at low Rayleigh numbers using a hybrid grid. Their results for the mean Nusselt numbers at steady state agree fairly well with those of Kuehn and Goldstein [1]. Genceli [13] presented experimental data for the onset of convection in water around a horizontal cylinder subjected to a constant surface heat flux. A critical Rayleigh number which defines the onset of convection was reported. Most recently, Song [14] published some numerical results of transient natural convection around a horizontal wire under a constant

NOMENCLATURE

D	cylinder diameter
g	gravitational acceleration
h	local heat transfer coefficient
k	fluid thermal conductivity
L	dimensionless radial distance between cylinder surface and outer boundary of solution domain
Nu	Nusselt number, hD/k
p'	pressure
Pr	Prandtl number, μ/α
q''	surface heat flux
r	dimensionless radial coordinate, r'/D
r'	radial coordinate
Ra	Rayleigh number, $g\beta D^3(T'_w - T'_\infty)/\mu\alpha$
Ra^*	modified Rayleigh number, $g\beta q'' D^4/k\alpha\mu$
t	dimensionless time, $t'\alpha/D^2$ (* signifies steady state almost attained)
t'	time
T	dimensionless temperature
T'	temperature
T'_w	temperature of cylinder surface
T'_∞	temperature of ambient fluid
u	dimensionless radial velocity, UD/α
U	radial velocity, positive outwards
U^*	modified dimensionless radial velocity, $UD/(\alpha\, Ra^{0.25})$
v	dimensionless angular velocity, VD/α
V	angular velocity, positive counterclockwise
V^*	modified dimensionless angular velocity, $VD/(\alpha\, Ra^{0.5})$
Y	radial distance from cylinder surface
Y^*	$(Y\, Ra^{0.25})/D$.

Greek symbols

α	thermal diffusivity
β	coefficient of thermal expansion
δ_T	thickness of the thermal boundary layer
δ_v	thickness of the viscous layer
θ	angular coordinate; zero is downward vertical, positive counter-clockwise on right half of cylinder
μ	kinematic viscosity
τ	time scale for the form of the thermal boundary layer
τ_d	delay time
Ψ	dimensionless stream function
Ω	dimensionless vorticity.

Superscript

$\bar{}$	average value.

Subscripts

i, j	nodal positions in the radial and angular directions, respectively.

heat flux using a finite difference method. His study however, was carried out only at low Rayleigh numbers ($0.12 < Ra^* < 20$). Furthermore, a physically unrealistic boundary condition imposed at the outer limit (i.e. $T = 0$ at $r = \infty$) of his computational domain would probably lead to numerical difficulties at high Rayleigh number computations.

To the authors' knowledge, transient solutions of the complete Navier–Stokes and energy equations for high Rayleigh numbers have not yet been reported. It appears that the primary difficulty to be overcome by the numerical procedure is the manner in which the outer (artificially imposed) boundary conditions, particularly the thermal condition at the outflow boundary of the plume is to be specified. A commonly used condition for the steady-state problem is to assume that the temperature gradient normal to the pseudo boundary is zero, thus implying that the heat transfer is dominated by convective movement rather than by conduction [1]. This obviously requires that the outflow velocities are sufficiently large, a condition that is probably satisfied within the scope of the steady-state case, since the plume region is fully developed. For the transient case however, before the full development of the plume, the validity of this assumption is not at all obvious.

Consequently, the present investigation is devoted to the numerical simulation of the transient laminar natural convection flow about a finite horizontal cylinder for a complete range of Rayleigh numbers using the spline method presented in ref. [4]. The advantages of this technique are that a variable grid spacing may be used, thus obviating the need for hybrid grids with their attendant interpolations; it is of high accuracy; requires fewer grid points for a given problem and can therefore be used on a personal computer. In addition, due to the various formulations possible, i.e. using the variable, its first derivative or its second derivative as the 'operational variable', higher order boundary conditions can be easily incorporated into the numerical scheme [15]. Computational results have been obtained for a range of Rayleigh numbers between 0.1 and 2×10^7.

GOVERNING EQUATIONS

The natural convection flow from a horizontal cylinder is governed by the continuity equation, the two-dimensional Navier–Stokes equation and the energy equation. In cylindrical polar coordinates, they take the following form:

continuity

$$\frac{\partial u'}{\partial r'} + \frac{u'}{r'} + \frac{1}{r'}\frac{\partial v'}{\partial \theta} = 0 \tag{1}$$

momentum, in the radial (r) direction

$$\frac{\partial u'}{\partial t'} + u'\frac{\partial u'}{\partial r'} + \frac{v'}{r'}\frac{\partial v'}{\partial \theta} - \frac{v'^2}{r'} = \frac{1}{\rho}\frac{\partial p'}{\partial r'} - g\cos\theta[1-\beta(T'-T'_\infty)] + \mu\left(\frac{\partial^2 u'}{\partial r'^2} + \frac{1}{r'}\frac{\partial u'}{\partial r'} + \frac{u'}{r'^2} + \frac{1}{r'^2}\frac{\partial^2 u'}{\partial \theta^2} - \frac{2}{r'^2}\frac{\partial v'}{\partial \theta}\right) \tag{2}$$

momentum, in the circumferential (θ) direction

$$\frac{\partial v'}{\partial t'} + u'\frac{\partial v'}{\partial r'} + \frac{v'}{r'}\frac{\partial v'}{\partial \theta} + \frac{u'v'}{r'} = \frac{1}{\rho r'}\frac{\partial p'}{\partial \theta} + g\sin\theta[1-\beta(T'-T'_\infty)] + \mu\left(\frac{\partial^2 v'}{\partial r'^2} + \frac{1}{r'}\frac{\partial v'}{\partial r'} + \frac{v'}{r'^2} + \frac{1}{r'^2}\frac{\partial^2 v'}{\partial \theta^2} + \frac{2}{r'^2}\frac{\partial u'}{\partial \theta}\right) \tag{3}$$

energy

$$\frac{\partial T'}{\partial t'} + u'\frac{\partial T'}{\partial r'} + \frac{v'}{r'}\frac{\partial T'}{\partial \theta} = \alpha\left(\frac{\partial^2 T'}{\partial r'^2} + \frac{1}{r'}\frac{\partial T'}{\partial r'} + \frac{1}{r'^2}\frac{\partial^2 T'}{\partial \theta^2}\right). \tag{4}$$

The non-dimensional equations in stream function and vorticity form (using the Boussinesq approximation for the body forces) may be written as

$$\nabla^2 \Psi = -\Omega \tag{5}$$

$$\frac{\partial \Omega}{\partial t} + u\frac{\partial \Omega}{\partial r} + \frac{v}{r}\frac{\partial \Omega}{\partial \theta} = Pr\,\nabla^2\Omega + Pr\,Ra\left(\sin\theta\frac{\partial T}{\partial r} + \cos\theta\frac{1}{r}\frac{\partial T}{\partial \theta}\right) \tag{6}$$

$$\frac{\partial T}{\partial t} + u\frac{\partial T}{\partial r} + \frac{v}{r}\frac{\partial T}{\partial \theta} = \nabla^2 T \tag{7}$$

with

$$\nabla^2 = \frac{\partial^2}{\partial r^2} + \frac{1}{r}\frac{\partial}{\partial r} + \frac{1}{r^2}\frac{\partial^2}{\partial \theta^2} \tag{8}$$

and

$$u = \frac{1}{r}\frac{\partial \Psi}{\partial \theta}, \quad v = -\frac{\partial \Psi}{\partial r}. \tag{9}$$

Boundary conditions

Since the flow is symmetric about a vertical plane passing through the axis of the cylinder, only the half-plane need be considered. The boundary conditions then become

$$u = v = \Psi = 0$$

$$\Omega = -\frac{\partial^2 \Psi}{\partial r^2}$$

and

$$T = 1$$

or

$$\frac{\partial T}{\partial r} = -1$$

on the cylinder surface and

$$\Psi = v = \Omega = \frac{\partial T}{\partial \theta} = 0 \tag{10}$$

on the lines of symmetry.

At the inflow region ($u < 0$)

$$v = \frac{\partial \Psi}{\partial r} = 0 = T, \quad \Omega = -\frac{1}{r^2}\frac{\partial^2 \Psi}{\partial \theta^2} \tag{11}$$

on the outflow region ($u > 0$)

$$v = \frac{\partial \Psi}{\partial r} = 0, \quad \Omega = -\frac{1}{r^2}\frac{\partial^2 \Psi}{\partial \theta^2}. \tag{12}$$

For the temperature boundary condition, attempts were made to develop a modified relation that may better express the intrinsic feature of the transient flow, without success. In the present study therefore, the commonly used boundary condition for outflow, i.e. a zero temperature gradient normal to the pseudo boundary has been adopted

$$\frac{\partial T}{\partial r} = 0. \tag{13}$$

Fortunately, numerical tests indicated [4] that during the transient state at higher Rayleigh numbers when the outflow boundary is far enough away from the cylinder surface, its influence on both the heat transfer and fluid flow near the surface of the cylinder is negligible, and the convection effects always dominate over conduction so that the latter can be usually neglected. A detailed discussion of this point will be presented in a forthcoming report.

NUMERICAL CONSIDERATIONS

The spline fractional step method (SFSM) [5] was used to generate an algorithm resulting in a tri-diagonal system containing either function values or first derivatives at the grid points. The essential feature of this method is that at each computational step, the problem is treated as a one-dimensional case in implicit form so that only one tridiagonal matrix system needs to be evaluated. The SFSM schemes representing the governing equations (5)–(7) and the boundary condition imposed at the outer circular limit have been reported in detail in ref. [4] and will therefore not be elucidated further.

RESULTS AND DISCUSSION

Scale analysis

Before solving equations (5)–(7) numerically, it is useful to rely on pure scaling arguments to theoretically predict the types of flow and heat transfer patterns that can develop near the cylinder surface. The scale analysis follows that due to Patterson and Imberger [16] for the natural convection flow in a rectangular cavity.

Immediately after the start of heating ($t' = 0$), the fluid bordering the cylinder surface is motionless, so that the energy equation (4) expresses a balance between thermal inertia and conduction normal to the cylinder surface. Taking $\Delta T'$, t' and $\delta_{T'}$ as the scales of changes on T', t' and the radial coordinate r' in equation (4) and assuming $\partial^2 T'/\partial r'^2 \gg \partial^2 T'/\partial\theta^2$ and $r' \gg \delta_{T'}$, the following relation may be obtained from equation (4):

$$\frac{\Delta T'}{t'} \sim \alpha \frac{\Delta T'}{\delta_{T'}^2}. \tag{14}$$

So

$$\delta_{T'} \sim (\alpha t')^{0.5}. \tag{15}$$

The heated layer $\delta_{T'}$ will naturally tend to rise along the cylinder wall. As in ref. [17] the velocity scale of this tangential motion may be obtained from the two momentum equations (2) and (3) by eliminating the pressure and retaining the dominant terms. For $Pr > 1$ (marginally valid for $Pr \simeq 1$ [17]), from the balance between buoyancy force and viscous force, the initial tangential velocity scale is

$$v' \sim \frac{g\beta\alpha\Delta T' \sin\theta}{\mu} t'. \tag{16}$$

Comparing with the vertical velocity scale for the rectangular cavity [16], it may be seen that the difference arises just in the term $\sin\theta$ inside the coefficient, since the dependence of tangential velocity will obviously depend on position θ.

The buoyancy forces act to accelerate the fluid only over the thickness $\delta_{T'}$; heat is being convected into this layer by the tangential velocity equation (16), and the layer will continue to grow until the heat conducted in from the boundary balances that convected away. For the present case, the convection term is of the order of $(\bar{v}'\Delta T'/R\pi)$ and the conduction term is of the order of $(\alpha\Delta T'/\delta_{T'}^2)$, thus

$$\frac{\bar{v}'\Delta T'}{R\pi} \sim \frac{\alpha\Delta T'}{\delta_{T'}^2} \tag{17}$$

or

$$\bar{v}'\Delta T'\delta_{T'} \sim \frac{\alpha\Delta T'}{\delta_{T'}} R\pi.$$

This relation, in fact, expresses the above balance. Here $\bar{v}'$ represents the average tangential velocity

$$\bar{v}' = \frac{1}{\pi}\int_0^\pi v'\,\mathrm{d}\theta \sim \frac{2}{\pi}\frac{g\beta\Delta T'\alpha}{\mu} t'.$$

From equation (16) we obtain

$$t' \sim \frac{\pi D^2}{2\alpha} Ra^{-0.5}$$

and

$$\delta_{T'} \sim \left(\frac{\pi}{2}\right)^{0.5} D\, Ra^{-0.25}$$

or in dimensionless form

$$\tau \sim \frac{\pi}{2} Ra^{-0.5} \tag{18}$$

and

$$\delta_T \sim \left(\frac{\pi}{2}\right)^{0.5} Ra^{-0.25}. \tag{19}$$

Here, τ represents the time scale of the thermal boundary layer formed. It is interesting to note that this time scale differs by a factor of $\pi/2$ over that ($\tau \sim Ra^{-0.5}$) for a rectangular cavity with height D and horizontal length D. This is because the fluid particles move along the cylinder surface in the boundary layer.

For the case of the constant heat flux surface boundary condition, taking into account the relation $Ra^* = Ra\,Nu$ and the correlation $Nu = 0.800(Ra^*)^{0.175}$ [3], the following relation may be obtained from equation (18):

$$\tau \sim 1.4(Ra^*)^{-0.413}. \tag{18'}$$

The viscous layer is governed by an inertial-viscous balance. From equation (3), the thickness of the viscous layer is about the order of $(\mu^{0.5}t^{0.5})$, i.e.

$$\delta_v \sim \mu^{0.5}t^{0.5} \tag{20}$$

thus

$$\delta_v \sim Pr^{0.5}\,\delta_T \tag{21}$$

which is the same relation as for a rectangular cavity [16].

Numerical solution

Numerical results have been obtained for various boundary conditions. In this paper, due to space limitations, the transient flow and temperature fields and heat transfer results will be discussed principally for the isothermal surface boundary condition although some computations for the constant heat flux case have also been presented.

The time dependent non-linear coupled partial differential equations were solved by considering an $(r$–$\theta)$ grid 11×21, 21×23, or 17×31 on a non-uniform mesh with $r_{i+1}/r_i = 1.30$ and $\theta_{j+1}/\theta_j = 0.87$ or $r_{i+1}/r_i = 1.10$ and $\theta_{j+1}/\theta_j = 0.91$ or $r_{i+1}/r_i = 1.15$ and $\theta_{j+1}/\theta_j = 0.93$, respectively. Near the cylinder surface and in the plume region, a very fine grid spacing was

chosen. (The angular coordinate θ is measured from the lower symmetry line, positive counterclockwise on the right half of the cylinder.) The change from inflow to outflow is computed automatically as in ref. [4] with no special assumption being required. The time step used in the present calculation was, in general, $\Delta t = 10/Ra$ for the vorticity and energy equations while the stream function equation was solved in false transient form.

Small time solution. At time $t = 0$, the temperature at the surface is increased suddenly from T_∞ to T_w and maintained at this value. Heat is transferred initially by pure conduction to the surrounding medium and for all Rayleigh numbers, this initial conductive phase is characterized by concentric circles for the isotherms in the axial plane, until a certain critical time is reached. Figures 1 and 2 show a typical sequence of the different stages of development at $Ra = 10$ (low Rayleigh number) and 10^7 (high Rayleigh number). Patterns similar to Fig. 1 have been observed in experiments using a heated wire [7]. For comparison with the experimental data of Genceli [13], a corresponding numerical solution compatible with a cylinder diameter of 25 mm was obtained with $Ra^* = 745\,000$ and $\alpha = 1.43 \times 10^{-7}$ for water at an ambient temperature of 20°C. The isotherm patterns are presented in Fig. 3 for different times. They are in very good agreement with Genceli's photographs using interferometry. According to equation (18′), for the present case $t_c' \sim 22$ and $R_c \sim 20$ (his definition). Comparing the present results with the experiments of ref. [13], the present results have been computed at times slightly advanced with respect to the experiments, as shown in Fig. 3.

A comparison between the present results and the experimental temperature profiles [13] at the top of the cylinder is presented in Fig. 4. The agreement is very good for specific values of critical delay time as well as for the development stage. However, beyond this critical period, a transient region is subsequently

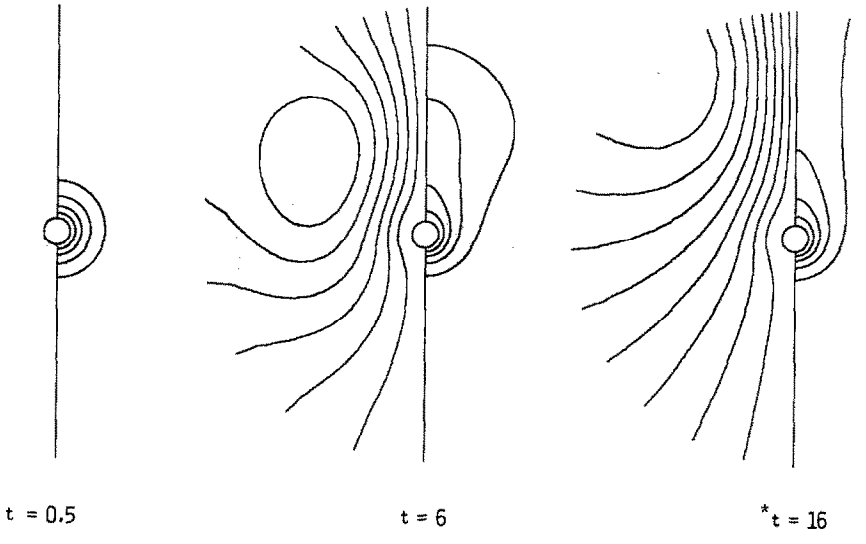

FIG. 1. Isotherms (right) and streamlines (left) at different stages of development for $Ra = 10$ and $Pr = 0.7$ ($\Delta\Psi = 1$ and $\Delta T = 0.1$).

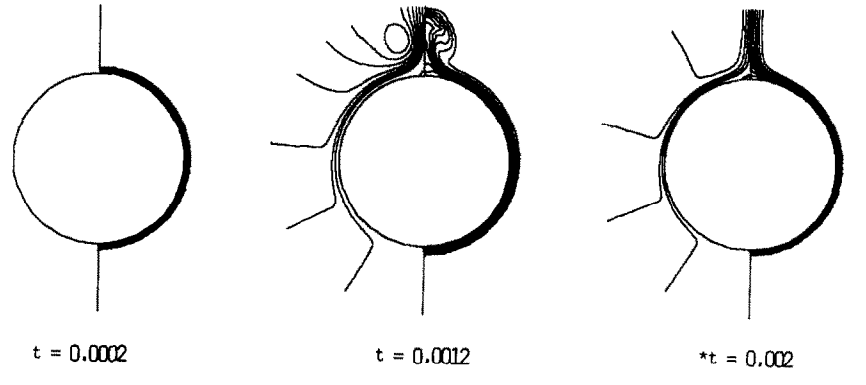

FIG. 2. Isotherms (right) and streamlines (left) at different stages of development for $Ra = 10^7$ and $Pr = 0.7$ ($\Delta\Psi = 20$ and $\Delta T = 0.1$).

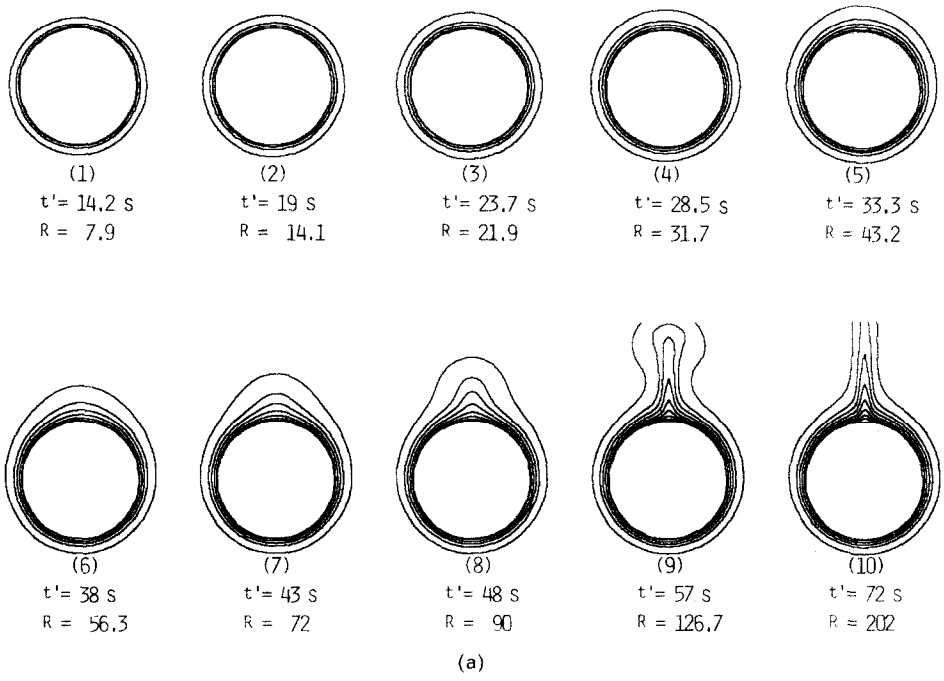

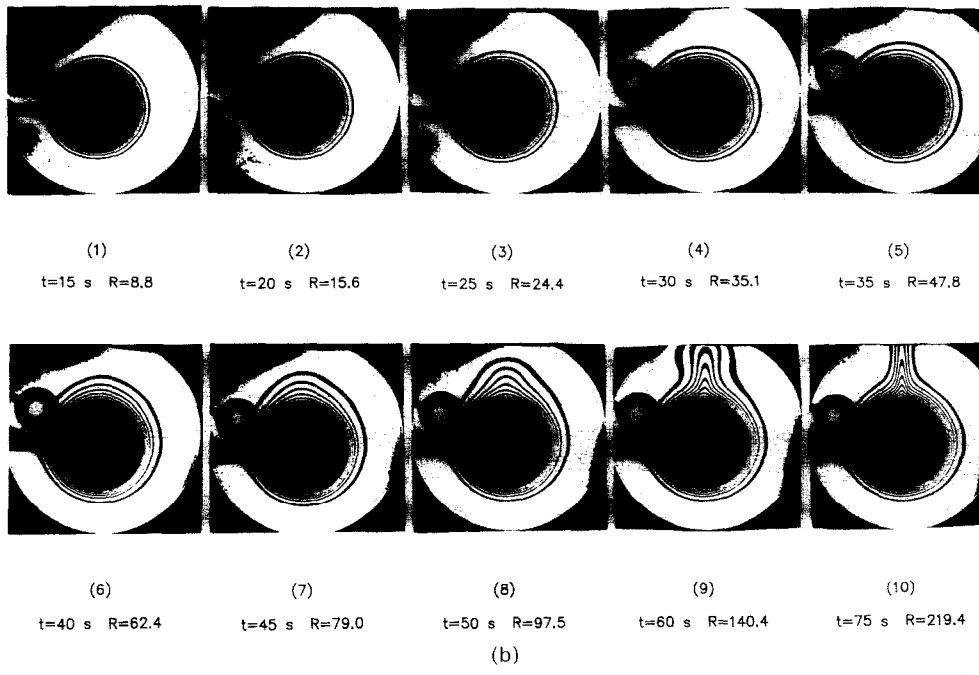

FIG. 3. (a) Isotherms at different stages of development for $Ra^* = 745\,000$ and $Pr = 7.01$ ($\Delta T = 0.2$). (b) Corresponding experiment from ref. [13].

formed with convective effects where particles start rising towards the top of the cylinder. This phenomenon has also been observed in the experiments of Parsons and Mulligan [8] and this period of time called the 'delay time' is denoted by τ_d. Numerical tests indicate that the value of τ_d is slightly greater than the τ obtained from a scale analysis. Furthermore, when $t \simeq \tau$, the thermal boundary layer thickness at first reaches its equilibrium (steady state) value (except for the plume region); then overshoots to a slightly greater thickness (attained at $t = \tau_d$) and finally backs down to its steady-state position. This phenomenon becomes more accentuated at low Rayleigh numbers. For example, the variation of tem-

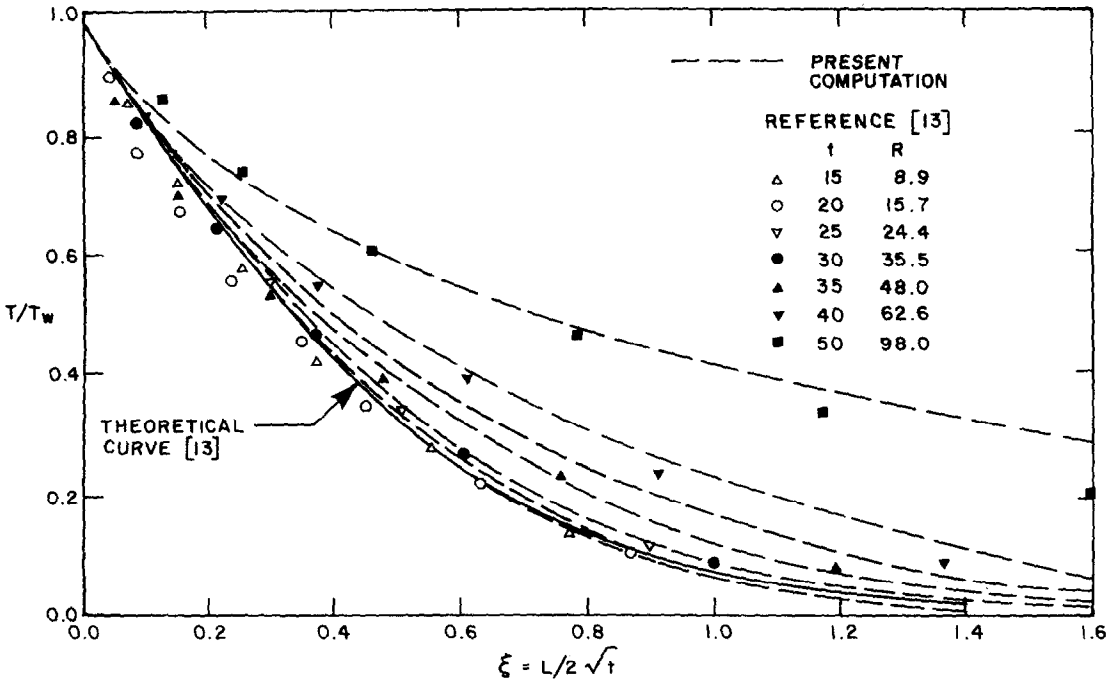

FIG. 4. Comparison between numerically computed and experimentally measured temperature profiles [13] at the top of the cylinder.

perature profiles at different times for $\theta = 90°$ and $Ra = 10$ is exhibited in Fig. 5(a). It is clearly seen that the temperature profile at a dimensionless time of $t = 0.9$ first approaches its steady-state thickness, then subsequently overshoots to its maximum value at about $t = 3.5$ while the corresponding average Nusselt number on the cylinder surface attains its minimum value (Fig. 5(b)), and then finally becomes thinner at the steady state. (This behaviour has also been observed by Parsons and Mulligan [8] at low Rayleigh numbers who call it the 'overshoot' of the steady state.)

Figure 6 indicates the comparison between the boundary layer solutions of ref. [12] and the present results for the tangential velocity profiles at $\theta = 90°$ for $Ra = 10^6$. (The parameter t'^* has been defined in ref. [12] as $2(2Pr\ Ra)^{0.25}t^{0.5}$.) The radial temperature

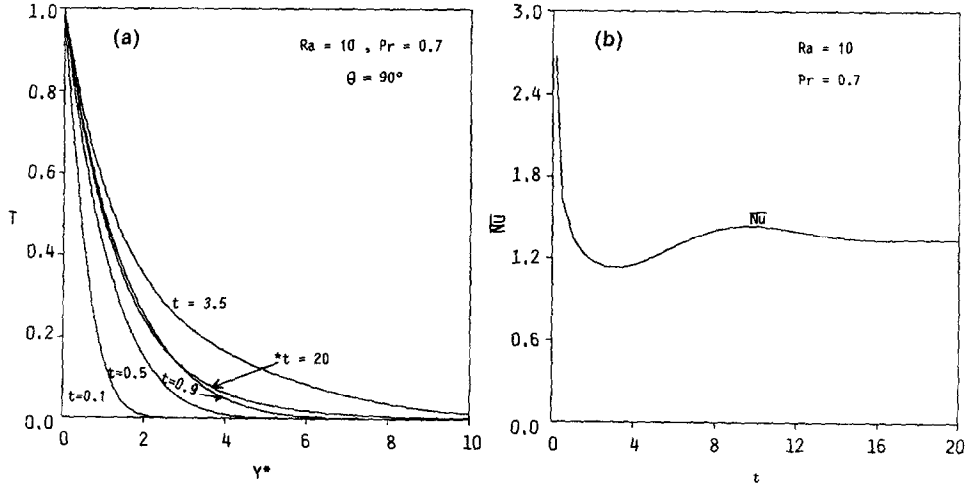

FIG. 5. For $Ra = 10$ and $Pr = 0.7$ at $\theta = 90°$: (a) radial temperature distribution at various times; (b) time histories of Nusselt numbers.

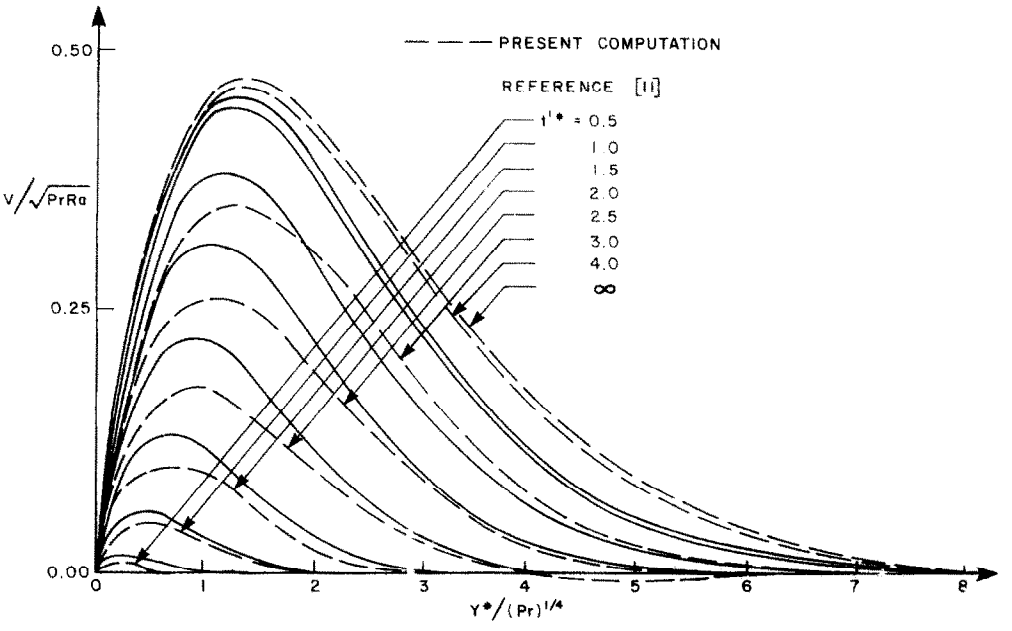

FIG. 6. Computed tangential velocity profiles compared with boundary layer results for $Ra = 10^6$, $Pr = 0.7$ and $\theta = 90°$ at various times.

profiles at $\theta = 0°$ are found to be virtually indistinguishable from those in ref. [12] and have not been reproduced here. However, the marked difference between the velocity profiles at small times is hardly surprising, since it is well known that the boundary layer assumptions break down when the viscous boundary layer is weak or nonexistent.

It is interesting to note that for $Ra = 10^6$ the thermal boundary layer was formed when $t \sim 0.0018$. This value coincides with that of τ from the scale analysis (in fact, $\tau \sim \pi/2Ra^{-0.5} \sim 0.0016$). For $Ra = 10^5$ and 10^7, the time taken to form the thermal boundary layer is about $t \sim 0.005$ and 0.00056, respectively, which compares favourably with the corresponding values from a scale analysis of $\tau \sim 0.0049$ and 0.0005. These results demonstrate that equation (18) obtained from the scale analysis, is a reliable guide in predicting the duration of the transient time of the pure conduction stage for higher Rayleigh numbers.

The overshoot phenomenon. Figures 7(a) and (b) are the profiles of temperature and tangential velocity for different times at $\theta = 132°$ and $Ra = 10^5$. The 'overshoot' behaviour is more evident and it is easy to see that the fluid particles rotate while rising. The negative V^* at large values of Y^* in Fig. 7(b) implies just such a recirculation.

It is important to note that for higher Rayleigh numbers the 'overshoot' phenomenon is strong in the region $120° < \theta < 170°$. Particularly for $Ra = 10^7$, the maximum 'overshoot' occurs near $\theta = 160°$. At this stage, the diffusion of heat from the surface dominates over any convective effects so that the buoyancy forces act to accelerate only the fluid within the narrow thermal region δ_T. Once convection starts however, fresh fluid is entrained into the heated region so that its temperature is reduced with an accompanying reduction in body forces. The overshoot behaviour is therefore most likely caused by fluid inertia effects. In order to further ascertain the details of the initiation of the convection regime, numerical experiments using particle trajectories were performed. The results (to be discussed later) indicate that as soon as the temperature of the cylinder surface is raised from T_∞ to T_w, particles adjoining the cylinder surface at $\theta = 90°$ commence moving and follow a path approximately tangential to the surface of the cylinder until they approach the top ($\theta = 180°$) where they separate and form a weak recirculating vortex region as shown in Figs. 1 and 2. It must be emphasized that during this whole transient process, the velocities involved are extremely low. Interestingly, the expected movement of fluid particles near the top of the cylinder occurs at $t > \tau$, that is, the development of the plume region lags behind the formation of the thermal boundary layer. This means that the onset of motion results from the natural convection along the approximately vertical portions of the cylinder surface near $\theta = 90°$ and not from a Bénard type convective instability in the statically unstable conduction temperature profile near $\theta = 180°$.

The development of the plume region. The development of the plume region is presented in further detail for $Ra = 10^6$ in Fig. 8. With the progress of time, convective effects become increasingly dominant. When $t > \tau$, i.e. after the boundary layer has formed, the tangential velocity continues to increase. This increase in convection causes development of the plume region. The upward flow along

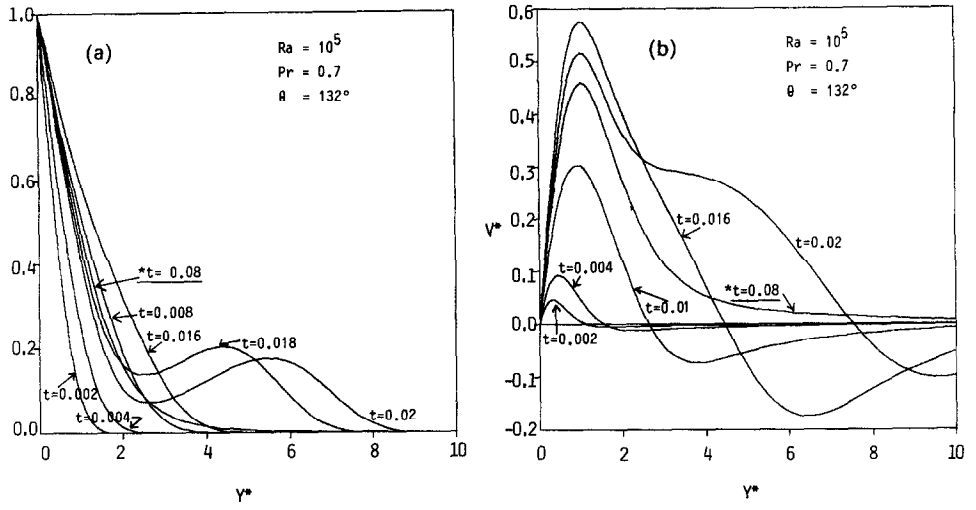

FIG. 7. Numerical results for $Ra = 10^5$, $Pr = 0.7$ and $\theta = 132°$: (a) radial temperature distribution at various times; (b) tangential velocity profiles at various times.

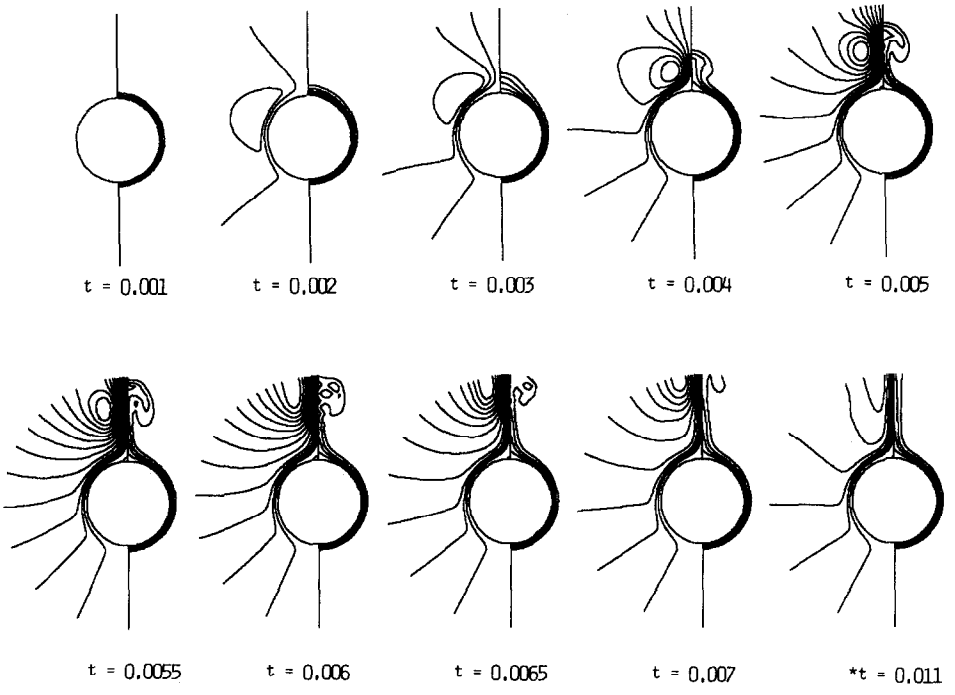

FIG. 8. Transient isotherms and streamlines for $Ra = 10^6$ and $Pr = 0.7$ ($\Delta\Psi = 10$ and $\Delta T = 0.2$).

the surface of the cylinder transports heated fluid to the top of the cylinder and gradually forms a distinct temperature front between the heated fluid and the unheated ambient as shown in Figs. 2 and 8. At the transient stage, the fluid at the top of the cylinder detaches itself and rises while rotating at the same time because of viscous effects. At a higher Rayleigh number, the rotation is quite evident and the leading edge of the heated fluid forms a 'mushroom' pattern which gradually degrades into the final (steady) state form of a convection plume. At very high Rayleigh number (about $Ra = 5 \times 10^7$), small separation vortices, symmetrically disposed near the top surface of the cylinder are formed, grow moderately, are shed

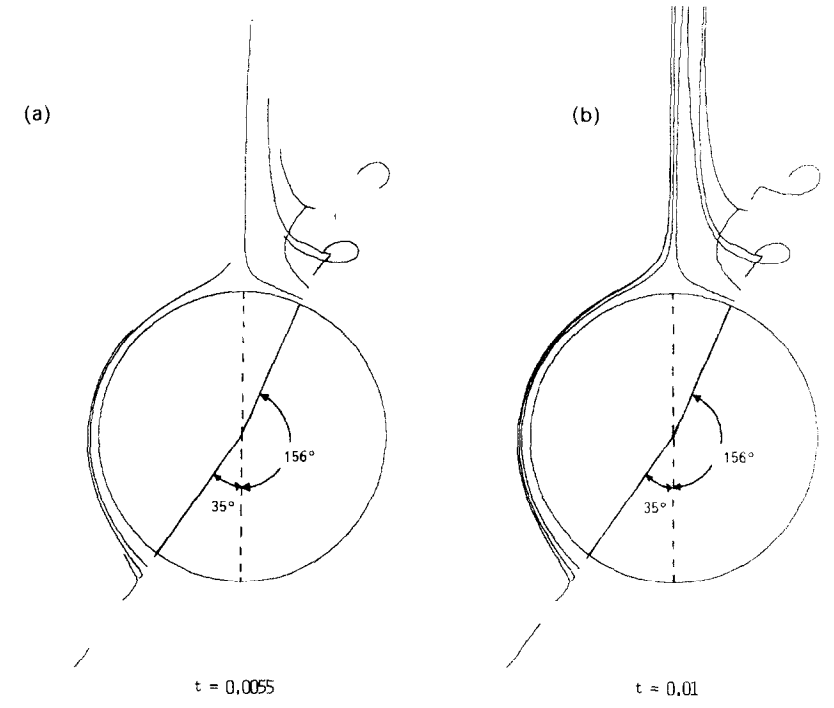

FIG. 9. Particle trajectories at different times for $Ra = 10^6$: (a) $t = 0.006$; (b) $t = 0.01$.

into the plume and then reformed again with this sequence repeating itself. (At the present time, it is unclear whether this rather interesting behaviour is due to deficiencies in the model (the use of a symmetric half-plane for example) or whether it is a physically realistic phenomenon.)

The particle trajectories presented in Fig. 9 provide other means with which to analyse the development of the fluid patterns for $Ra = 10^6$. For low Rayleigh numbers ($Ra < 10$), particles rise with almost no rotation anywhere. However, at higher Rayleigh numbers, particles which initially are within the region of $90° < \theta < 270°$ (except inside the boundary layer and at the vertical line) rise while rotating simultaneously. For example, trajectories of particles initially placed along a radial line at $\theta \simeq 156°$ are presented in Fig. 9. It is interesting to note that particles close to the cylinder surface have fairly stable paths after they are entrained into the boundary layer as shown in the left half of the figure (at the line $\theta \simeq 325°$ or $\theta = 35°$). These trajectories are in basic qualitative agreement with experimental observations [6].

Local and average Nusselt numbers. The time variation of local surface Nusselt numbers for $Ra = 10^4$, 10^5 and 10^6 is shown in Figs. 10 and 11(a) and (b). For $Ra = 10^4$, comparison between the present results and those of Sako *et al.* [12] are presented. The agreement is quite good.

In general, at the initial stage, the local Nusselt numbers are uniformly distributed since heat transmission is by conduction. With time, convection begins to set in so that for $Ra = 10^6$ at $t = 0.0012$, the maximum difference between the Nusselt numbers is about 20% indicating that convective effects are becoming significant. Finally at steady state, there is about a 84% difference between the value of Nu at the top and at the bottom of the cylinder. The 'overshoot' behaviour although present, is less marked than that at low Rayleigh number.

The time variation of the mean Nusselt numbers at the cylinder surface for different Rayleigh numbers is presented in Fig. 12. For lower Rayleigh numbers they are in good agreement with the results presented in ref. [12], however, due to space limitations they have not been reproduced here. Since the cylinder surface temperature increases suddenly from T_∞ to T_w, the starting heat transfer coefficients are initially large, then decrease quickly as the thickness of the thermal region grows until it reaches its minimum value and then increases again until it gradually attains its steady state. The lower the Rayleigh number, the more pronounced is the 'overshoot'. For example, values range from about 17% of steady state at $Ra = 1$ to about 2% for $Ra = 10^7$. After the 'overshoot' and before attaining a steady state, the values of Nu at the higher Rayleigh numbers suffer very small oscillations that are almost impossible to detect in the figures. It is possible that this effect is caused by fluid inertia effects that lag behind the body forces driving them, so that the steady state of even the velocity field is attained in an oscillatory manner and not in smooth monotonic fashion.

For lower Rayleigh numbers, a boundary layer cannot be formed and convection is relatively weak, so

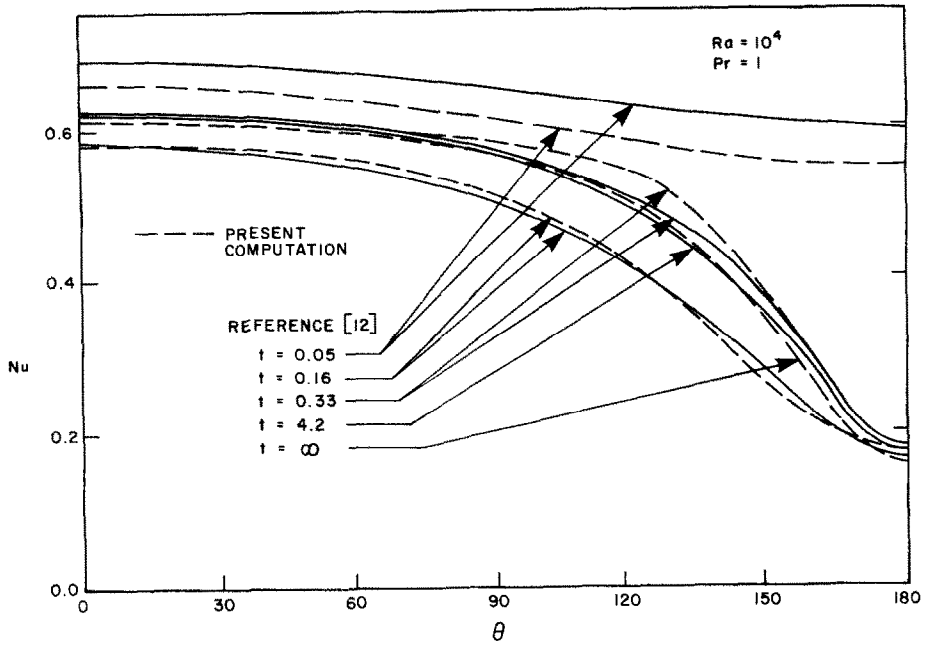

FIG. 10. Comparison between the present solution and those of ref. [12] for local heat transfer coefficients at $Ra = 10^4$ at different times.

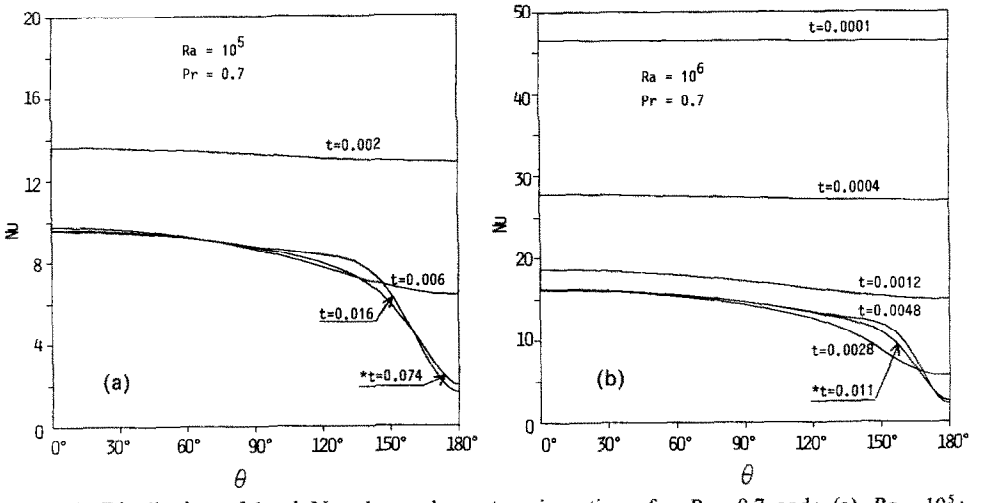

FIG. 11. Distribution of local Nusselt numbers at various times for $Pr = 0.7$ and: (a) $Ra = 10^5$; (b) $Ra = 10^6$.

that conduction effects are dominant except far away from the cylinder surface. However, at higher Rayleigh number, the effect of conduction is in general, limited to the boundary layer; outside this layer convection effects are always dominant.

The influence of Prandtl number Pr on Nu is shown in Fig. 12(a) for $Ra = 10^5$. The higher the Prandtl number, the higher the value of the Nusselt numbers.

Variation of surface vorticity. Figures 13(a) and (b) show the time variation of the vorticity distribution on the cylinder surface for $Ra = 10^6$ and 10^7, respectively. For higher Rayleigh numbers, the 'overshoot' phenomenon is strong in the range of $120° < \theta < 170°$ instead of in the range of $90° < \theta < 150°$ [11] observed at lower Rayleigh numbers. It is evident that an increase in Ra causes not only an increase in the value of the vorticity but also causes the range of the 'overshoot' to shift towards the vertical. It is interesting to note that at the initial stage, the surface vorticity increases everywhere, however after a certain time ($t > \tau$) the values of vorticity decrease quickly in the range of $170° < \theta < 180°$ for $Ra \geqslant 10^5$, this decrease becoming more pronounced the higher the

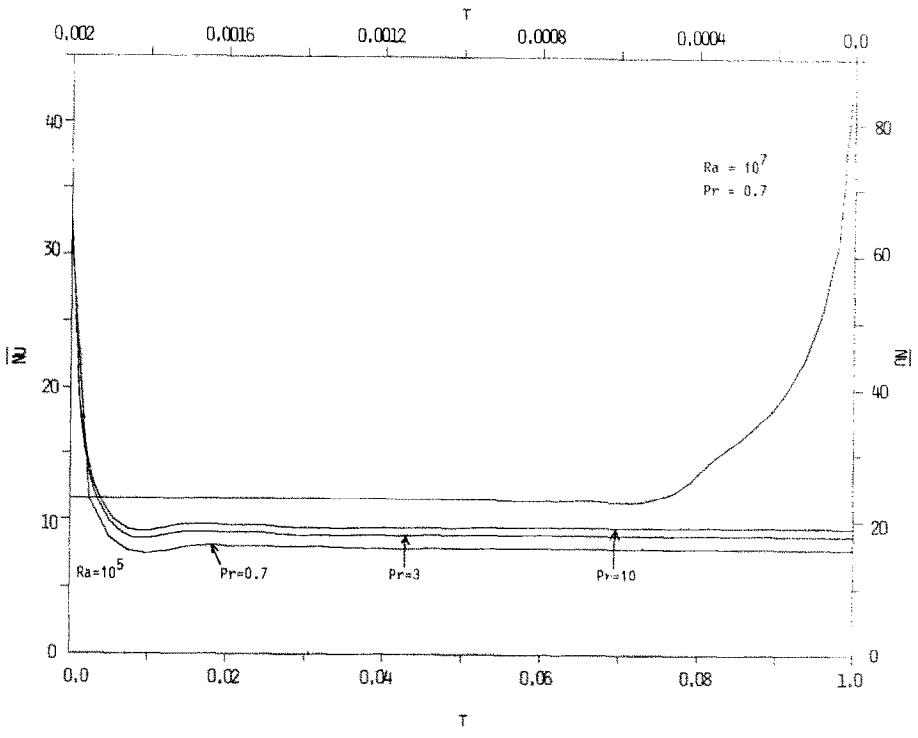

FIG. 12. Time histories of $\overline{Nu}$ for various Rayleigh numbers: (a) $Ra = 10^5$ and $Pr = 0.7$, 3 and 10; (b) $Ra = 10^7$ and $Pr = 0.7$.

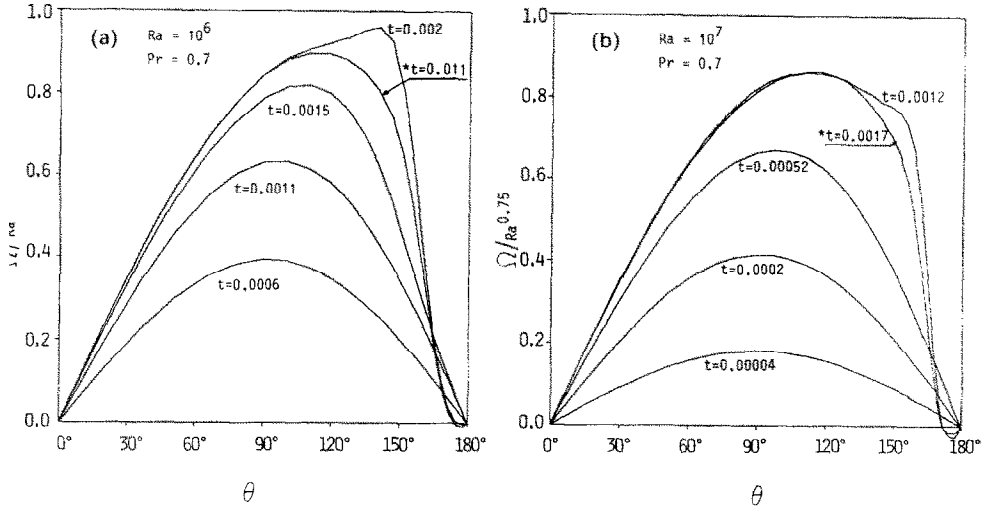

FIG. 13. Surface vorticity distribution at various times for $Pr = 0.7$ and: (a) $Ra = 10^6$; (b) $Ra = 10^7$.

Rayleigh number. When $Ra \geqslant 10^6$ a counter-rotating vortex is formed near the top of the cylinder. This appears to be due to the following causes: on the one hand in the region near the top of the cylinder the heat transfer is relatively low so that the buoyancy force and therefore the rise velocity associated with it becomes quite weak; on the other hand when $Ra \geqslant 10^6$ the convection becomes very strong and results in a local heated region close to the surface near $\theta = 170°$ so that a horizontal inverse temperature gradient (which may be a direct cause of the counter-rotating vortex) is formed. When $Ra > 5 \times 10^7$ the final steady counter-rotating vortex cannot be obtained, however the phenomenon where it forms, is then shed and reforms has been observed. It has also been noted that at high Rayleigh numbers, under constant heat flux or small Biot number surface boundary conditions, the counter-rotating vortex may be formed in the transient stage, but finally disappears, since the heat transfer coefficients near the top

of the cylinder are relatively large compared with the isothermal case.

Instability. A rather interesting numerical feature has been observed during the development of the plume region. For high Rayleigh numbers, for example $Ra \geqslant 10^6$, the plume flow behaves in a laminar fashion below a certain characteristic distance measured vertically from the top of the cylinder. However, beyond this distance, the temperature distribution exhibits some oscillations, indicated in Fig. 8 ($t = 0.006$), that can eventually cause instability in the numerical procedure. In particular, for Rayleigh numbers exceeding 10^7 at large values of the dimensionless distance L (for example, $L > 1$), difficulties were encountered in attempts to obtain a convergent numerical solution. This is possibly a prelude to the development of the transition from laminar flow to turbulence.

CONCLUSIONS

The transient natural convection from a circular, horizontal cylinder has been studied numerically using spline integration techniques. Good agreement with published experimental and numerical data has been obtained. Overshoot and oscillatory behaviour of the local Nusselt numbers have been observed which decay as the steady state is approached. This has been associated with fluid inertia effects. At high Rayleigh numbers, the appearance of separation vortices, which are subsequently formed, shed and reformed when $Ra > 5 \times 10^7$, has been noted.

Acknowledgement—The authors gratefully acknowledge the assistance of one of the reviewers who brought refs. [11, 13] to their attention. We would also like to express our gratitude to Dr O. F. Genceli who kindly provided us with the original photographs for Fig. 3(b). This work was supported by the Natural Sciences and Engineering Research Council of Canada under Grant Numbers OGP0008846 and OGP0036586.

REFERENCES

1. T. H. Kuehn and R. J. Goldstein, Numerical solution to the Navier–Stokes equations for laminar natural convection about a horizontal isothermal circular cylinder, *Int. J. Heat Mass Transfer* **23,** 971–979 (1980).
2. B. Farouk and S. I. Guceri, Natural convection from a horizontal cylinder—laminar regime, *J. Heat Transfer* **103,** 522–527 (1981).
3. Z. H. Qureshi and R. Ahmad, Natural convection from a uniform heat flux horizontal cylinder at moderate Rayleigh numbers, *Numer. Heat Transfer* **11,** 199–212 (1987).
4. P. Wang, R. Kahawita and T. H. Nguyen, Numerical computation of the natural convection flow about a horizontal cylinder using splines, *Numer. Heat Transfer* **17,** Part A, 191–215 (1990).
5. P. Wang, Spline method of fractional steps in numerical model of unsteady natural convection flow at high Rayleigh number, *Numer. Heat Transfer* **11,** 95–118 (1987).
6. G. A. Ostroumov, Unsteady heat convection near a horizontal cylinder, *Sov. Tech. Phys.* **1,** 2627–2641 (1956).
7. C. M. Vest and M. L. Lawson, Onset of convection near a suddenly heated horizontal wire, *Int. J. Heat Mass Transfer* **15,** 1281–1283 (1972).
8. J. R. Parsons, Jr. and J. C. Mulligan, Transient free convection from a suddenly heated horizontal wire, *J. Heat Transfer* **100,** 423–428 (1978).
9. L. Elliott, Free convection on a two-dimensional or axisymmetric body, *Q. J. Mech. Math.* **23,** 153–162 (1970).
10. A. S. Gupta and I. Pop, Effects of curvature on unsteady free convection past a circular cylinder, *Physics Fluids* **20,** 162–163 (1977).
11. M. Katagiri and I. Pop, Transient free convection from an isothermal horizontal circular cylinder, *Wärme- und Stoffübertr.* **12,** 73–81 (1979).
12. M. Sako, T. Chiba, J. M. S. Garza and A. Yanagida, Numerical solution of transient natural convective heat transfer from a horizontal cylinder, *Jap. Heat Transfer* 24–44 (1982).
13. O. F. Genceli, The onset of manifest convection from suddenly heated horizontal cylinders, *Wärme- und Stoffübertr.* **13,** 163–169 (1980).
14. Y. W. Song, Numerical solution of transient natural convection around a horizontal wire, *J. Heat Transfer* **111,** 574–576 (1989).
15. P. Wang and R. Kahawita, Numerical integration of partial differential equations using cubic splines, *Int. J. Comput. Math.* **13,** 271–286 (1983).
16. J. Patterson and J. Imberger, Unsteady natural convection in a rectangular cavity, *J. Fluid Mech.* **100,** 65–86 (1980).
17. A. Bejan, *Convection Heat Transfer.* Wiley, New York (1984).

CONVECTION NATURELLE LAMINAIRE VARIABLE AUTOUR DE CYLINDRES HORIZONTAUX

Résumé—La convection naturelle laminaire variable autour d'un cylindre chaud horizontal avec diverses conditions aux limites est étudiée numériquement en utilisant une méthode spline à échelons fractionnels. Quelques caractéristiques de la couche limite, obtenues avec une analyse d'échelle, sont comparées aux résultats numériques. On évalue le développement de la région de panache aussi bien que le champ local d'écoulement et le transfert thermique en surface. Pour les temps petits, les solutions numériques approchent les résultats de la couche limite et elles sont en bon accord avec les résultats de l'analyse d'échelle. On fait une étude détaillée du développement de la région de panache en utilisant des trajectoires calculées de particules. Tous les résultats ont été obtenus en utilisant un calculateur personnel. Des comparaisons qualitatives entre les résultats de calcul et les visualisations d'écoulement vérifient partiellement les résultats numériques.

ZEITLICH VERÄNDERLICHE LAMINARE NATÜRLICHE KONVEKTION AN EINEM WAAGERECHTEN ZYLINDER

Zusammenfassung—Die instationäre laminare natürliche Konvektion an einem beheizten waagerechten Zylinder wird numerisch mit Hilfe des Spline-Schrittverfahrens für verschiedene Randbedingungen an der Oberfläche untersucht. Einige Eigenschaften der Grenzschicht, die mit Hilfe einer Abschätzung der Größenordnung ermittelt worden sind, werden mit numerischen Ergebnissen verglichen. Die Entwicklung der Auftriebsfahne wie auch der Wärmeübergang an der Oberfläche und das örtliche Strömungsfeld werden berechnet. Für kleine Zeiten nähern sich die numerischen Ergebnisse denjenigen der Grenzschichtlösung. Sie stimmen in diesem Fall gut mit den Ergebnissen aus der Größenordnungsabschätzung überein. Das Gebiet der Auftriebsfahne wird unter Verwendung berechneter Partikelbahnkurven eingehender untersucht. Sämtliche Ergebnisse beruhen auf Berechnungen mit einem Personal-Computer. Ein qualitativer Vergleich zwischen den vorliegenden Ergebnissen und experimentellen Strömungsbeobachtungen bestätigt teilweise die numerischen Ergebnisse.

ПЕРЕХОДНЫЙ РЕЖИМ ЛАМИНАРНОЙ ЕСТЕСТВЕННОЙ КОНВЕКЦИИ ВОЗЛЕ ГОРИЗОНТАЛЬНЫХ ЦИЛИНДРОВ

Аннотация—С использованием сплайнового метода дробных шагов численно исследуется нестационарное ламинарное естественноконвективное течение от нагретого горизонтального цилиндра при различных граничных условиях на поверхности. Некоторые характеристики пограничного слоя, полученные при анализе размерностей, сравниваются с численными результатами. Оцениваются развитие области восходящего потока, а также поверхностный теплоперенос и локальные характеристики поля течения. При малых интервалах времени найденные численные решения приближаются к результатам, полученным в приближении пограничного слоя, и хорошо согласуются с результатами анализа размерностей. Более детально описывается развитие области восходящего потока на основе рассчитанных траекторий частиц. Все результаты получены на персональном компьютере. Качественные сравнения полученных данных и экспериментов по визуализации течения частично подтверждают достоверность численных результатов.